CERN'S BULK NIOBIUM HIGH GRADIENT SRF PROGRAMME: DEVELOPMENTS AND RECENT COLD TEST RESULTS

A. Macpherson*, K. Hernandez Chahin, C. Jarrige, P. Maesen,
F. Pillon, K.-M. Schirm, R. Torres-Sanchez, N. Valverde Alonso.
CERN, Geneva, Switzerland

Abstract

Recent results from the bulk niobium high-gradient cavity development program at CERN are presented, with particular focus on test results for the 704 MHz bulk niobium 5-cell elliptical cavity prototypes produced for the Superconducting Proton Linac (SPL) project. Successive cold tests of bare cavities have been used to refine the cavity preparation and testing process, with all steps done in-house at CERN. Current performance results are discussed with reference to observables such as ambient magnetic field, field emission levels, and quenches.

INTRODUCTION

As part of CERN's ongoing programme of accelerator development, an R&D programme on bulk Niobium cavities has been established, with the focus on achievement of high gradients for elliptical cavities. For this programme, the work is a follow-on from the SPL project [1], and is designed to update the in-house competencies in superconducting RF, but also put in place the necessary infrastructure. Over the last 2 years, significant investment has occurred, with an ISO4 cleanroom and high pressure water rinsing facility, refurbished vertical and horizontal test-stand cryostats, and new measurement and diagnostic capabilities coming online.

Using the SPL 5-cell bulk niobium $\beta = 1$ elliptical cavities designed with a fundamental TM mode frequency at 2K of 704.4MHz as the primary test structures (see Fig. 1), a series of cold tests have been conducted to validate the SPL cavity RF performance. As part of this process, cavity surface preparation, measurement and analysis have also been improved. The SPL cavities specifications require an operating acceleration gradient of 25 MV/m with a $Q_0 = 1.0 \times 10^{10}$ at 2K, and the challenge has been to achieve this level of performance. Four prototype cavities have been produced in industry and two have been tested to date.

EXPERIMENTAL SETUP

Surface preparation and vertical testing of the cavity prototypes has been done entirely at CERN, including high pressure rinse, bakeout and assembly, with all but the chemistry being done in CERN's recently commissioned SRF cleanroom facility [2]. Vertical cold tests were performed in CERN's SM18 4 m deep vertical cryostat, and a summary of the RF surface preparation steps are:

- Degreasing by submersion in a NetInox solution

---

* alick.macpherson@cern.ch

- Bulk electro-polishing: average removal of 160 µm
- 650 °C bake for 12 hrs then 12 hrs cool down
- Final electro-polishing: average removal of 20 µm
- High Pressure Rinsing, in a 100 bar rinsing cabinet.
- Drying in ISO4 clean room in laminar air flow.
- Assembly in an ISO4 cleanroom environment
- Mounting on the cryostat insert and leak testing
- [OPTIONAL] Bakeout at 120 °C for 40 hrs
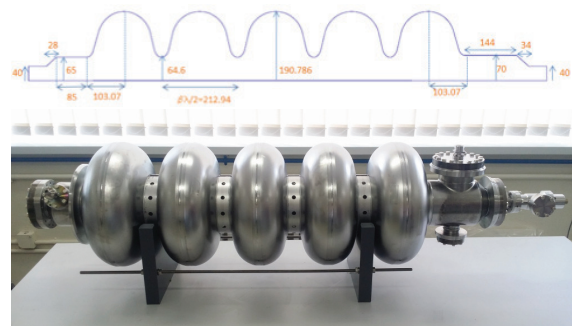- Cool down to 2 K: ambient magnetic field below 30 nT.

Figure 1: Mechanical dimensions of the $\beta = 1$ SPL cavity and a photo of the assembled cavity ready for testing.

Electropolishing of the first prototype (SPL1) was done with a simple solid body copper cathode, resulting in a surface containing numerous pinhole defects and shallow grooves. Both defects are understood in terms of excessive surface contact of hydrogen gas bubbles during the electropolishing process, with the former seen as a potential source of field emmission sites. For this reason the electropolishing cathode was redesigned with a mesh structure to allow improved flow through the cavity [3]. The second prototype (SPL2) was electropolished with the redesigned cathode. As can be seen from Fig. 2 the redefined cathode produced a much improved surface that was visibly free of pinholes and grooves.

High pressure rinsing of the cavities is done with a vertical 100 bar High Pressure Rinsing (HPR) cabinet with di-jet nozzle. A standard HPR rinse is composed of 6 cycles, each taking 50 min and is with a vertical nozzle speed of 0.5 mm/s, and a cavity rotation of 3 RPM.

Standard monitoring and diagnostic systems are deployed on the cavity; these include a 30 sensor OST array, 18 channels of temperature monitoring using contact temperature resistors (CERNOX, RuO_2, and Allen Bradley), cavity and Helium bath pressure gauges, and 3 single axis magnetic flux probes for ambient magnetic field measurement. The fully instrumented insert can be seen in Fig. 3.

(a) SPL1: Near Equator   (b) SPL1: Near Iris
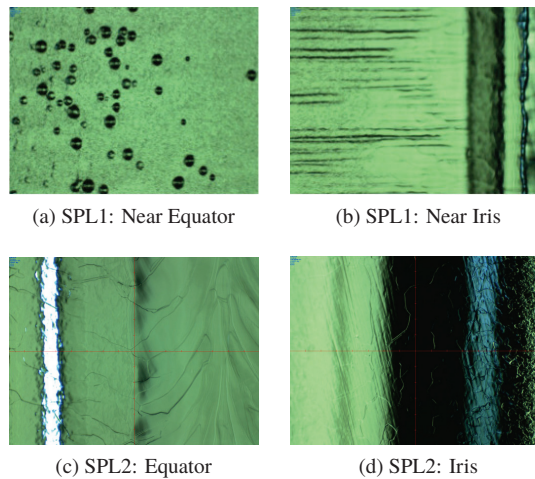
(c) SPL2: Equator   (d) SPL2: Iris

Figure 2: Visual inspection of the prototype cavities prior to testing. SPL1 electro-polished using a solid copper cathode, and SPL2 using a flow optimised copper mesh cathode.
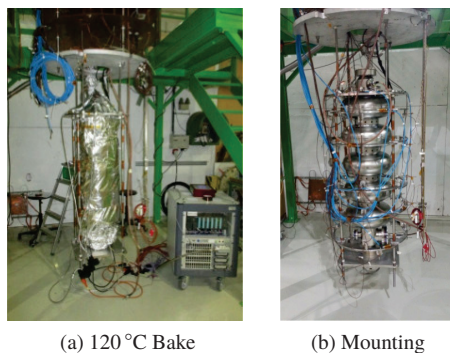

(a) 120 °C Bake   (b) Mounting

Figure 3: Preparation of the cavity insert prior to installing in the vertical cryostat.

CAVITY PERFORMANCE

Measurement of cavity performance of the two SPL prototypes has been done in a progressive and systematic study over the last calendar year, as both expertise and infrastructure evolved, and an overview of the cold tests that have been preformed is given in Table 1 and Fig. 4.

For the SPL1 prototype, improvement in the low field Q_0 was attributed to the optimisation and repetition of the high pressure rinse step. Going from a light HPR (Case A - with an HPR vertical nozzle speed of $3\,\mathrm{mm\,s^{-1}}$) where the low Q_0 implied a residual resistance of $R_{Res} = 19.7\,\mathrm{n\Omega}$), to our standard HPR (CaseB), a significant improvement in surface cleanliness was achieved, with $R_{Res} = 12.2\,\mathrm{n\Omega}$. Repeated HPR after a light BCP further improved R_{Res} to $9.5\,\mathrm{n\Omega}$.

Similarly, accelerating gradient showed progressive improvement due to both surface cleanliness and changes in the experimental conditions. Comparison of Case B and C suggest that control of the trapped magnetic flux at the superconducting transition shows a moderate improvement in the mid to high field Q-drop. Likewise, the effect on Q-drop of a 36 hour 120 °C bakeout on the cavity can be seen in the comparison of Case B and D. Such a bakeout

is typically expected to reduce mid field Q-drop, but here only a moderate benefit is observed, and so at this stage the benefits of the 120 °C bake are seen as marginal.

As part of the operational procedure, care has been taken to control the cavity cool down. To avoid excessive formation of niobium hydrides and the onset of Q-disease in the 100 K to 50 K, the cryostat volume is rapidly cooled from 300 K to 15 K without stopping and typical cool down rates are of order 15 K/min. With such a rapid cool down, large spatial thermal gradients on the cavity (in excess of 200 K) are observed, which create large thermal-electric currents over the cavity length. These are seen as variations in the ambient magnetic field, as measured by fluxgate monitors mounted 2 cm away from the cavity surface (see Fig. 6).

Once the bottom of the cavity has reached 15 K, cooling is stopped, and the cavity thermalised before compensating the ambient magnetic field prior to cooling through T_c. The ambient magnetic field is set by three independent compensation coils external to the cryostat, with the maintainable magnetic field less than 30 nT (see Fig. 6). With both the ambient magnetic field and the spatial temperature gradient controlled, a superconducting transition with a spatial thermal gradient at transition of less than 0.5 K over the entire cavity can be achieved. However, a spatial thermal gradient of less than 0.5 K at T_c and a cool down speed of 1 K/min has been used in order that the phase transition sweeps over the length of the cavity, and the amount of trapped magnetic flux limited, as evidenced by the small (30 nT) increase in the measured ambient magnetic field (see Fig. 6).

In terms of RF performance the influence of uncompensated ambient magnetic field was considered in Case E, F, and G, where the ambient magnetic field prior to cooling down through T_c was set at less than 10 nT, 40 μT, and 7 μT respectively (with all non-negligible magnetic field components in the cavity axis direction). The effect of the unsuppressed magnetic field is strikingly evident, with Case G showing degraded Q_0 and accelerating gradient reach, while the effectively unshielded case (Case F) gave extremely poor performance (as was expected) with $R_{Res} \approx 150\,\mathrm{n\Omega}$.
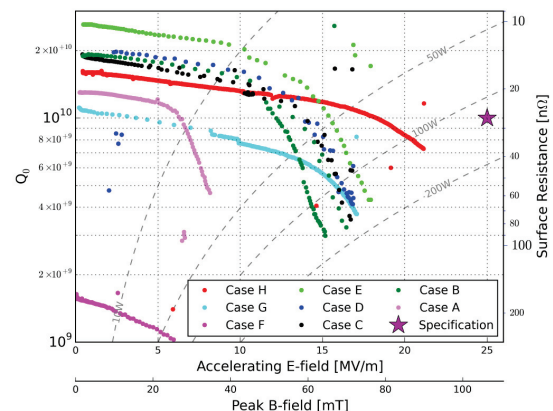

Figure 4: Comparison of the different cold test scenarios given in Table 1. Also shown on the plot are the contour lines of constant cavity power.

Table 1: Summary of Cavity Cold Tests for SPL the Prototype Cavities

|	Cavity	Surface Preparation	120 °C Bake	Thermal gradient control at T_c
Case A	SPL1	Limited HPR	Yes	Yes
Case B	SPL1	Standard HPR	No	No
Case C	SPL1	Unchanged from CaseB	No	Yes
Case D	SPL1	Unchanged from CaseB	Yes	No
Case E	SPL1	Light BCP of 20 μm + Standard HPR	No	Yes
Case F	SPL1	Unchanged from Case E + Ambient B-field at 40 μT	No	Yes
Case G	SPL1	Unchanged from Case E + Ambient B-field at 7 μT	No	Yes
Case H	SPL2	Standard HPR	No	Yes
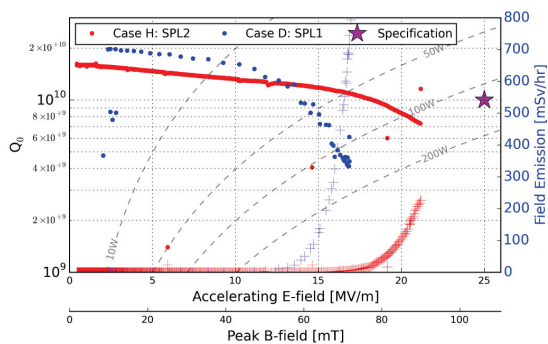
Figure 5: Comparison of the best cold test results for the two SPL prototype cavities at 2.06 K. Radiation levels are shown as marked with a " + ".
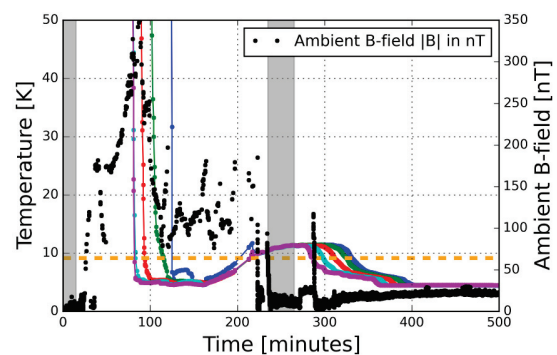

Figure 6: Expulsion of magnetic flux as the cavity is cooled through T_c. The grey bands show when the compensation coils feedback loop was on to compensate out the ambient magnetic field to < 30 nT.

Finally, and perhaps most significantly, the improvement in RF performance due to an improved electro-polishing a mesh design cathode [3] can be seen in the comparison of tests of the SPL1 and SPL2 prototype (Case E and H). SPL2 shows a significant improvement in RF performance, reaching a gradient of 21.7 MV/m with a $Q_0 = 7.2e9$. (alternatively, at a $Q_0 =1e10$, the E_{acc} was 18.2 MV/m), which represents a 20% improvement in gradient over the SPL1 prototype. In both cases, the high gradient reach was limited due to high levels of field emission, as can be seen in Fig. 5. Further, the onset of field emission moved from 12 to 16 MV/m, due primarily to the improved surface finishing from the new electro-polishing cathode [3]. In terms of field emission, the level of radiation, as measured immediately above the cryostat top-plate is well beyond acceptable levels for a cavity destined for a cryo module, implying further optimisation of surface preparation is still needed. It should be noted that for SPL1 the cavity only tripped due to localised heating of the beam port end flange from the "beam" of accelerated electrons generated by the field emission. For SPL2, the cavity reached the limit of the power system (due to the fixed input coupler) and only quenched due to global thermal loading after some time at the maximum power.

LORENTZ FORCE DETUNING

For the cold test measurement stand, the accuracy and precision of frequency tracking during measurement scans has been progressively improved such that for the test of the SPL2 prototype, realtime measurement of the Lorentz Force detuning of the cavity was possible. Lorentz force detuning is the shift in cavity resonant frequency due to the deformation of the cavity shape from radiation pressure generated by the cavity electromagnetic field, with the frequency shift Δf proportional to E_{acc}^2. From the SPL2 cold test (Case H) a detailed frequency tracking over the full scan (Fig. 7) shows the Lorentz force detuning with a detuning constant $K_L = -3.16 Hz/(MV/m)^2$. This should be compared with the specifications value of $K_L = -5 Hz/(MV/m)^2$ [1] for a free standing bare cavity.

QUENCHES AND SURFACE DEFECTS

With the high level of radiation observed during the testing of the SPL1 prototype, high power quenches were frequent, especially during conditioning. In order to better understand the source of the field emission, quench locations have been analysed using trilateration of second sound waves [4]. As
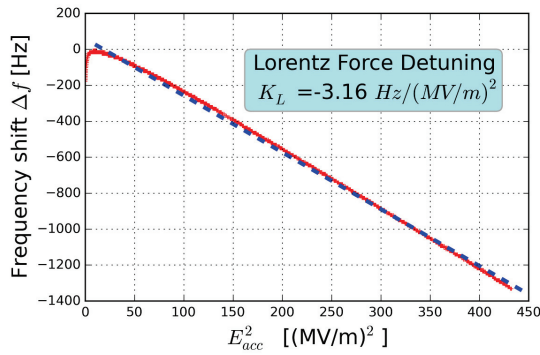
Figure 7: Lorentz force detuning relation from the SPL2 cold test. The red data points are realtime frequency tracking measurements taken during powering and the fit to the data is in blue.
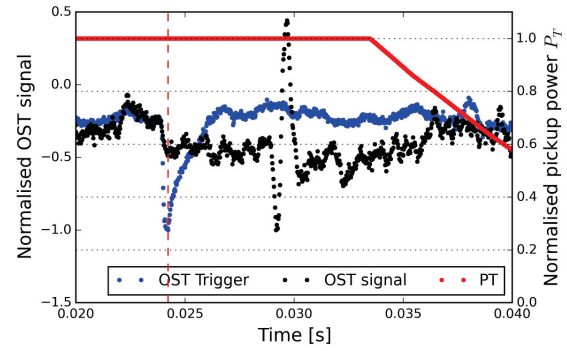

Figure 8: OST trigger (1st sound), a typical OST data signal (2nd sound) and transmitted power from a mid-field quench of the SPL1 prototype just after the turn -on of field emission.

second sound waves can be thought of as a relative density fluctuation of the He II:He I ratio, Oscillating Superleak Transducers (OST) were deployed to detect second sound waves within the cryostat. Further, only quenches occurring during the initial onset of field emission were considered, in order to avoid effects from thermal loading from high radiation levels associated with the the high-field quenches.

Figure 8 shows a typical OST signal from one such mid-field quench. For quench localisation by trilateration, correct triggering of the quench is required, and as seen from Fig. 8, the cavity power trip is not necessarily synchronised with the quench; for multi-cell cavities with localised quench spots well away from the cavity antennas, synchronisation mismatch is not uncommon. For proper triggering of the quench, several OST sensors constructed with a taut superleak film are used, as they appear sensitive to what appears to be 1st sound fluctuation that can be used as a prompt trigger. This, along with constant fraction discrimination of the OST signals provides a set of 2nd sound signals that can be used for trilateration. As with the method discussed in [5], the speed of second sound propagation is left as a free parameter, but unlike [5], the cavity surface is not used as a constraint on the trilateration.

From this second sound trilateration, the location of quench spot in the high field region of the second cell of SPL1 was predicted as a quench spot, and from post cold test optical inspection of the surface, a defect as shown in Fig. 9 was identified. The difference in coordinates between prediction and observed defect was $\Delta\theta = 1.9°$ and $\Delta z = 9.5mm$. While Fig. 9 is not an image of a textbook emitter, the fact that it was in a high B-field location of the cavity, and that the surrounding surface area was otherwise unremarkable lends to the veracity of the quench spot identification.

For additional insight into the field emission sources, Fowler-Nordheim modelling [6] [7] of field emission current for RF cavities has been used to estimate the effective area ($A_{emitter}$) and the associated field enhancement factor (β_{FE}) of the cavity emitters. This modelling can be written in terms of the DC dark current measured in the cavity pick-up, and the peak cavity surface electric field. The linear fit of
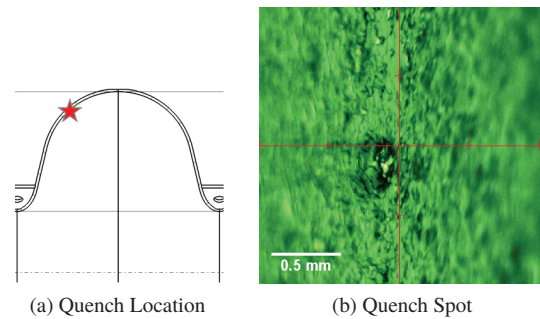

(a) Quench Location   (b) Quench Spot

Figure 9: Identified quench spot found by optical inspection.

the current and field measurements into a Fowler-Nordheim plot, $\ln(I/E^{2.5})$ vs $1/E_{peak}$, provides estimates for $A_{emitter}$ and β_{FE} are given by:

$$\beta_{FE} \propto \frac{1}{\text{Slope}_{FN}} \qquad A_{emitter} \propto \frac{1}{f}(\text{Slope}_{FN})^{2.5} e^{\text{Intercept}_{FN}}$$

For the SPL1 prototype, there is significant mid-field field emission (insert of Fig. 10), and a clear correlation between observed radiation and pickup antenna DC dark current. The resulting Fowler-Nordheim analysis gives emitter surface area and field enhancement vales compatible with similar cavity measurements [8]. Here it is assumed the pickup antenna operates as a Faraday cup, and collects all emitter dark current, which is unrealistic. However, as effective area scales inversely to fraction of dark current the pick-up observes, $A_{emitter} = O(\mu m)$ could be expected.

While it is difficult to extract useful information from this Fowler-Nordheim analysis to aid the identification of defects, it is encouraging to see that the effective emitter size after a light Buffer Chemical Polishing (BCP) increased by a factor ≈ 420, in line with the overall 'softening' of the geometrical profile of surface defects (ie reduction of the field enhancement factor and a broadening of emitter area). It should be also be noted that the non-linearity for Case D in Fig. 10 is a classic indication of multipacting [8].
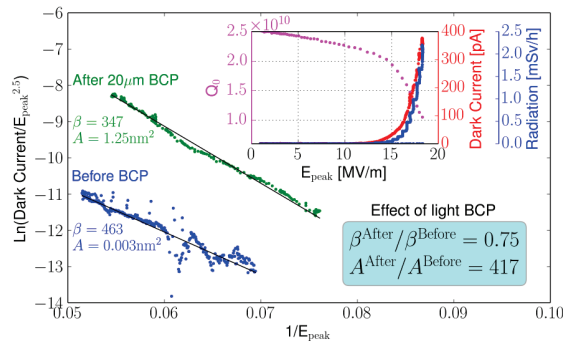
Figure 10: Fowler Nordheim plot from the SPL1 cavity for test Case D (blue) and Case E(green). The insert shows for Case D, the quality factor Q_0 (magenta), pickup antenna dark current (blue), and radiation from field emission (red).

Figure 11: Frequency shift as a function of temperature, to give the penetration depth, mean free path and RRR.

MATERIAL PROPERTIES

In order to understand the material properties of the prototype cavities, measurement of resonant frequency change as a function of temperature below T_c can be used to determine the change in penetration depth of the magnetic field, and from that the average electron mean free path and residual resistance ratio of the RF surface layer extracted [9]. For the 3400 litre vertical cryostat used at CERN, this measurement was extremely difficult to make as the large volume meant the measurement was overshadowed by frequency fluctuations from cryostat pressure variations. By addressing the cryostat operation procedure and by emptying the cryostat, pumping it down to a pressure 28 ± 0.3 mbar, and then slowly warming the cryostat an accurate tracking as the cavity uniformly warmed to T_c was possible (Fig. 11).

As shown in Fig. 11, the RRR determined this way for the SPL2 prototype was 11.8 nm, which, for a cavity that has been baked at $120\,^{\circ}\mathrm{C}$, is well below the typical bulk value of 250 to 300. The explanation of this low value has not yet been found, as the procedure has been shown to be good [10], but the either there is actually a low RRR layer sitting on the high RRR bulk due to a non uniform chemistry, or the possible surface contamination during the HPR. The latter is suspected due to the discovery of partial corrosion on the HPR nozzle made from 400 grade stainless steel that was not rated for 100 bar pressures with ultra-pure water.

CONCLUSION

Over the past year CERN's SRF high gradient program has made significant progress in its ability to prepare and test bulk Niobium cavities. Clear progress has been established with the 5-cell bulk niobium SPL cavities. The high gradient reach is still limited by field emission but work is ongoing to push the onset of field emission to higher gradients. This, coupled with strengthening of in-house expertise and techniques, as well as the validation of CERN SRF infrastructure suggest that SPL cavity prototypes can be pushed to their RF performance specification in the coming year, thus making them available for cryomodule assembly.
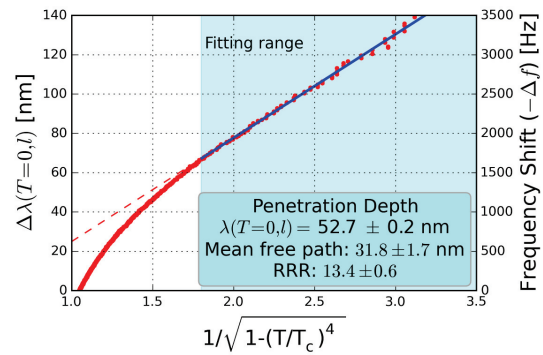
REFERENCES

[1] F. Gerigk and European Organization for Nuclear Research, *Conceptual design of the low-power and high-power SPL: a superconducting H- Linac at CERN*, CERN, 2014.

[2] J. Chambrillon, M. Therasse, O. Brunner, P. Maesen, O. Pirotte, B. Vullierme, and W. Weingarten, "CERN SRF assembling and test facilities", Proc. SRF11, Chicago, 2011.

[3] Leonel Ferreira, "Cathode Geometry and Flow Dynamics Impacton Vertical Electropolishing of Superconducting Niobium Cavities", MOPB100, *these proceedings*, Proc. SRF2015, Whistler, Canada (2015).

[4] Z. A. Conway, D. L. Hartill, H. S. Padamsee, and E. N. Smith, "Oscillating superleak transducers for quench detection in superconducting ILC cavities cooled with He-II", THP036, Proc. LINAC08, Victoria, BC, Canada (2008).

[5] T. Junginger et al., "High Flux Three Dimensional Heat Transport in Superfluid Helium and Its Application to a Trilateration Algorithm for Quench Localisation with OSTs," MOPB049, *these proceedings*, Proc. SRF2015, Whistler, Canada (2015).

[6] R.H. Fowler and L. Nordheim, "Electron Emission in Intense Electric Fields", Proceedings of the Royal Society A: Mathematical, Physical and Engineering Sciences **119**(781), 173 (May 1928).

[7] B. Bonin, "Field emission in RF cavities," CERN European Organization for Nuclear Research-Reports-CERN, pp. 221–230, 1996.

[8] K. Yoshida, J. Halbritter and M. Yoshioka, "Measurements of Superconducting Niobium Cavities at 700 MHz," IEEE Trans. Nucl. Sci. **26**, 4114 (1979).

[9] Gianluigi Ciovati, "Effect of low-temperature baking on the radio-frequency properties of niobium superconducting cavities for particle accelerators," Journal of Applied Physics, **96**(3), 1591 (2004).

[10] A Macpherson, K. Hernandez Chahin, C. Jarrige, P. Maesen, K.-M. Schirm, R. Torres-Sanchez, S. Aull, A. Benoit, P. Fernandez Lopez, R. Valera Teruel, and T. Junginger, "Diagnostic Developments at CERN's SRF Testing Facility", TUPB080, *these proceedings*, Proc. SRF2015, Whistler, Canada (2015).